ACS Catalysis

Research Article

Cite This: ACS Catal. 2019, 9, 11341−11349

pubs.acs.org/acscatalysis

Highly Selective Photocatalytic Valorization of Lignin Model Compounds Using Ultrathin Metal/CdS

Guanqun Han,[†] Tao Yan,[‡] Wei Zhang,[§,∥] Yi C. Zhang,[⊥] David Y. Lee,[⊥] Zhi Cao,*[,‡,§] and Yujie Sun*[,†]

[†]Department of Chemistry, University of Cincinnati, Cincinnati, Ohio 45221, United States

[‡]Syncat@Beijing, Synfuels China Co., Ltd, Beijing 101400, China

[§]State Key Laboratory of Coal Conversion, Institute of Coal Chemistry, Chinese Academy of Sciences, Taiyuan 030001, China

[∥]University of Chinese Academy of Sciences, Beijing, 100049, China

[⊥]Department of Chemistry and Materials Science & Engineering Program, Washington State University, Pullman, Washington 99163, United States

Supporting Information

ABSTRACT: Depolymerization of recalcitrant lignin is a crucial step in realizing the full potential of transforming biomass to value-added small organic molecules. Herein, we report a photocatalytic system consisting of ultrathin CdS nanosheets decorated with first-row transition metals (M/CdS) for the direct photocleavage of lignin model compounds to small aromatic products. In the meantime, the reducing power of M/CdS is utilized to simultaneously generate another valuable product, H_2, hence eliminating the necessity of sacrificial reagents and maximizing the energy conversion efficiency. We further demonstrate that, by judiciously modulating the photocatalytic conditions, it is feasible to yield different products with very high selectivity using the same catalyst of Ni/CdS. A series of control experiments were performed to investigate the mechanistic steps of each reaction and highlight the important roles played by both solvent and base in the photocleavage of the β-O-4 bond in lignin valorization.

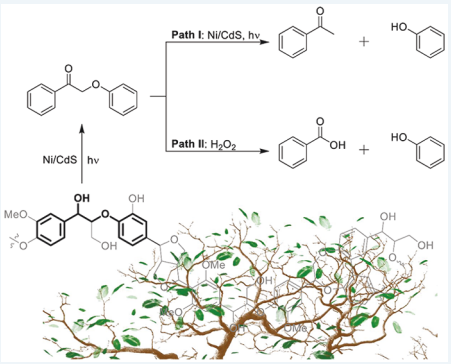

KEYWORDS: *lignin valorization, photocatalysis, selective photocleavage, ultrathin CdS, nickel cocatalyst*

INTRODUCTION

Upgrading biomass to produce value-added fuels and commodity chemicals has been considered as a sustainable and green approach in utilizing renewable carbon resources, complementary to the conventional chemical industry which heavily relies on fossil fuels, in that biomass consists of contemporary carbon whose utilization will not alter the CO_2 concentration in the atmosphere.[1−4] In this context, lignocellulosic biomass, including cellulose, hemicellulose, and lignin, has attracted increasing interest in biorefinery.[5−10] In particular, lignin is a highly functionalized biopolymer that can be transformed to small aromatics; however, its recalcitrant structure renders it challenging to be depolymerized.[11−13] The primary hurdle of lignin valorization is the selective and effective cleavage of those complex linkages connecting aromatic units in the lignin structure. One of the prevalent linkages is the β-O-4 bond which is estimated to constitute 43−65% of all lignin linkages.[14,15]

Because the homolytic bond dissociation enthalpy of C_β−O has been theoretically predicted to decrease from 69.2 to 55.9 kcal/mol once the benzylic C_α−OH group is oxidized to ketone,[16] a two-step β-O-4 cleavage pathway has been widely adopted for lignin depolymerization, wherein the oxidation of C_α−OH to ketone is followed by the break of the C_β−O bond.[17−19] Consequently, oxidative cleavage of lignin and its model compounds has been the subject of intensive investigation.[15] Nevertheless, the majority of reported methods require harsh conditions and expensive/toxic chemical oxidants with unsatisfactory yield and/or selectivity.[20] Along the theme of green chemistry, O_2 is a desirable oxidant owning to its low cost, large abundance, and benign nature. For instance, Stahl et al. reported an AcNH-TEMPO-mediated (AcNH-TEMPO = 4-acetamido-2,2,6,6-tetramethylpiperidine-*N*-oxyl) catalytic system for the cleavage of lignin models utilizing O_2 as the external oxidant for the first step, C_α−OH oxidation to ketone (Figure 1a).[21] Taking advantage of electricity and light, together with powerful hydrogen atom transfer mediators like *N*-hydroxyphthalimide (NHPI) and expensive Ir photocatalyst (i.e., $[Ir(ppy)_2(dtbbpy)](PF_6)$), Stephenson's group reported a one-pot, two-step strategy for the cleavage of lignin model compounds, electrocatalytic oxidation of benzylic alcohol followed by photocatalytic β-O-4 cleavage (Figure 1b).[22−24] However, the homogeneous nature of the above two catalytic systems makes the product

Received: July 5, 2019
Revised: October 31, 2019
Published: November 1, 2019

DOI: 10.1021/acscatal.9b02842
ACS Catal. 2019, 9, 11341−11349

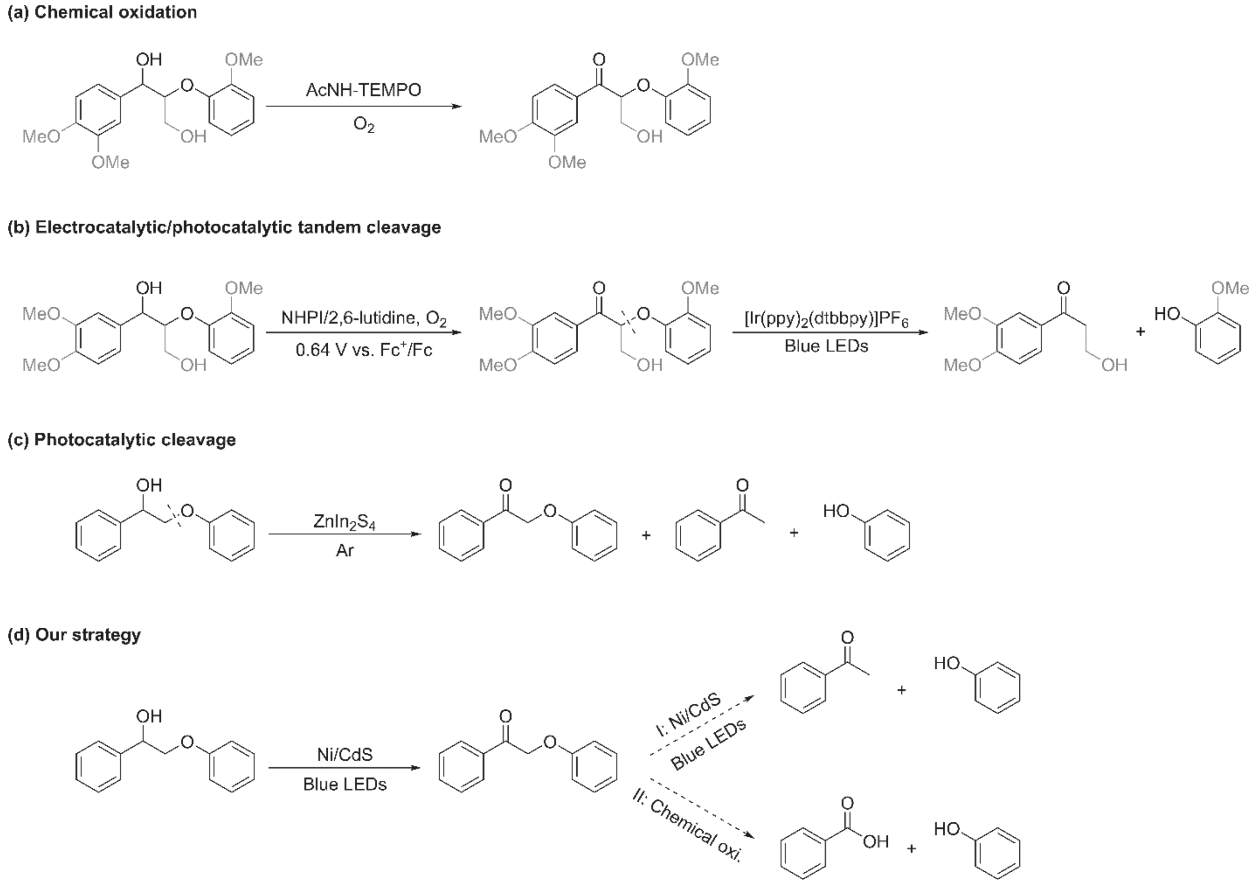

Figure 1. Reported oxidation and cleavage strategies of lignin model compounds and our proposed strategy of photocleavage with two possible pathways. (a) Chemical oxidation. (b) Electrocatalytic/photocatalytic tandem cleavage. (c) Photocatalytic cleavage. (d) Our strategy.

separation and purification challenging. In addition, the cost and long-term robustness of redox mediators (i.e., AcNH-TEMPO and NHPI) and Ir-based photocatalysts also question their applicability on a large scale. Compared to the aforementioned homogeneous catalytic systems, solid-state catalysts have been recognized with unique advantages such as easy separation and potential recyclability. A particularly attractive option is photocatalytic valorization on semiconductors.[25] As shown in Figure 1c, Wang et al. developed a transfer hydrogenolysis protocol for the photocatalytic valorization of lignin models on $ZnIn_2S_4$.[26] Although the ketone intermediate could be obtained, its yield is always quite low (32% in 1 atm O_2 atmosphere while in most cases less than 10%). In the meantime, the direct cleaved products of acetophenone and phenol could be detected with good to poor yields. Overall, this system lacks high selectivity for desirable products.

On the other hand, solar-driven H_2 production via semiconductor/cocatalyst systems is generally regarded as a promising approach in transforming and storing intermittent solar energy in H_2, in that H_2 is not only a clean fuel but also an important commodity chemical.[27,28] This process only utilizes excited electrons generated in semiconductors upon light irradiation. However, the excited holes will compete to recombine with excited electrons and a common strategy to mitigate charge recombination is to use sacrificial electron donors to quench those excited holes, which eventually wastes the oxidizing power of excited holes. A more desirable strategy is to make use of both excited electrons and holes for two valuable reactions. Within this context, it has become of increasing interest in coupling oxidative biomass valorization with concomitant H_2 production, which will not only eliminate sacrificial reagents, but also produce two types of value-added products with maximized photoenergy utilization. Our group has initiated a program focusing on this integrated photocatalysis strategy and recently reported the photocatalytic upgrading of biomass-derived HMF (5-hydroxymethyl furfural) to more valuable DFF (2,5-diformylfuran) with the coproduction of H_2 under ambient conditions.[29] Herein, we explore a library of cocatalysts decorated on two-dimensional (2D) ultrathin CdS nanosheets (M/CdS, M = Mn, Fe, Co, Ni, Cu) and achieve different products from the oxidative photocleavage of lignin model compounds in highly selective manners (Figure 1d).

RESULTS

Synthesis and Characterization of Photocatalysts M/CdS. Our ultrathin CdS nanosheets were obtained from the reaction between $CdCl_2$ and S in diethylenetriamine at 80 °C for 30 min under microwave irradiation. Subsequently, the resulting CdS nanosheets were mixed with common metal chloride salts and $NaBH_4$ to obtain the final M/CdS photocatalysts (M = Mn, Fe, Co, Ni, or Cu). Such a two-step microwave-assisted synthetic strategy enabled us to readily synthesize five different photocatalysts for a systematic study. Figure 2a compiles the X-ray diffraction (XRD) patterns of M/CdS as well as the pristine CdS. Compared to the standard XRD pattern (JCPDS 41-1049) of CdS, it is apparent that the

DOI: 10.1021/acscatal.9b02842
ACS Catal. 2019, 9, 11341−11349

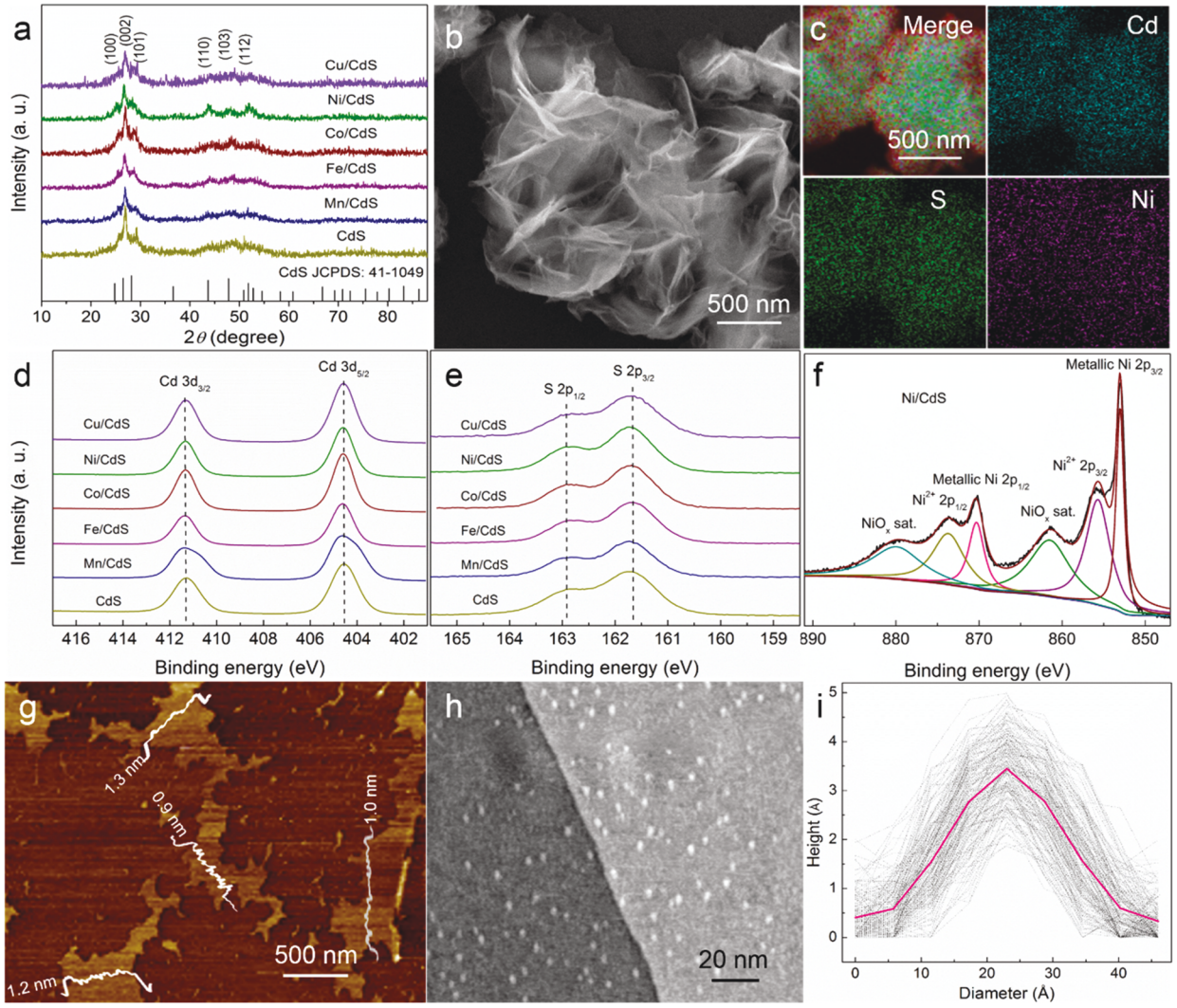

Figure 2. Characterizations of M/CdS. (a) XRD patterns of CdS and M/CdS together with the standard CdS JCPDS 41-1049. (b) SEM image of Ni/CdS. (c) Elemental mapping images of Ni/CdS. (d, e) High-resolution XPS spectra of Cd 3d (d) and S 2p (e) of M/CdS and CdS. (f) High-resolution XPS spectrum of Ni 2p of Ni/CdS. (g) AFM image of Ni/CdS with height profiles in selected areas. (h) STM image of Ni/CdS. (i) Height vs displacement cross sections of all the nickel species in Ni/CdS in Figure 2h.

decoration of first-row transition metals did not alter the crystal structure of each catalyst, which still maintained the wurtzite CdS structure. The relatively poor crystallinity of these samples was most likely due to their ultrathin thickness as discussed later. Inductively coupled plasma optical emission spectroscopy (ICP-OES) data were collected for all the M/CdS samples and the Ni weight percentage in Ni/CdS was ~5.0% (Table S1). The scanning electron microscopy (SEM) images of Mn/CdS (Figure S1), Fe/CdS (Figure S2), Co/CdS (Figure S3), Ni/CdS (Figure 2b and Figure S4), and Cu/CdS (Figure S5) were collected to confirm their nanosheet morphology. No apparent nanoparticles or aggregates were observed, implying the very small size of those decorated transition metals on CdS. Elemental mapping analysis also confirmed the identity and homogeneous distribution of Cd, S, and Ni in Ni/CdS (Figure 2c and Figure S6). Similar results could be obtained for the other four samples (Figures S7–S10). In line with the aforementioned characterization results, X-ray photoelectron spectroscopy (XPS) further verified the composition of anticipated elements in these photocatalysts, including Cd, S, and the corresponding transition metal (Figure S11). Figure 2d presents the high-resolution Cd 3d XPS spectra of all the samples including the bare CdS, wherein the two distinctive peaks at 411.4 and 404.6 eV can be attributed to the Cd $3d_{5/2}$ and $3d_{3/2}$ features, respectively.[30] For the S 2p spectra shown in Figure 2e, the two peaks at 162.8 and 161.7 eV correspond to S $2p_{3/2}$ and $2p_{1/2}$, respectively.[31] Again, the nearly identical Cd and S XPS spectra of M/CdS and CdS demonstrate that the decoration of transition metals on CdS does not substantially alter the valence states of both Cd and S. As an example, the high-resolution Ni 2p spectrum of Ni/CdS was plotted and fitted in Figure 2f. The three subpeaks at 853.0, 855.9, and 861.5 eV can be assigned to the metallic Ni $2p_{3/2}$, Ni^{2+} $2p_{3/2}$, and NiO_x $2p_{3/2}$ satellite peaks, respectively.[32,33] The other subset of peaks at 870.3, 873.7, and 880 eV is attributed to the Ni $2p_{1/2}$ features. The presence of oxidized nickel species is probably resulting from exposure to air during synthesis and posttreatment. The high-resolution metal 2p XPS spectra of other samples are included in Figure S12. Atomic force microscopy (AFM) measurement of Ni/CdS was conducted to confirm its ultrathin thickness. As shown in Figure 2g and Figure S13, the

DOI: 10.1021/acscatal.9b02842
ACS Catal. 2019, 9, 11341−11349

thickness of Ni/CdS was only ~1.2 nm with no apparent thickness change after nickel decoration. In order to determine the size of nickel species in Ni/CdS, scanning tunneling microscopy (STM) was performed. Figure 2h presents the STM image of Ni/CdS wherein those white spots with a diameter of a few nanometers can be attributed to the supported nickel. The height profile in Figure 2i demonstrates the average thickness and size of these nickel nanoparticles in Ni/CdS are ca. 0.3 nm and 3.5 nm, respectively. These observations are drastically different from that of the pristine CdS nanosheets which possess a very smooth surface (Figure S14).

Photocatalytic Oxidation of Benzylic Alcohol and Its Derivatives. Prior to the photocatalytic oxidation of lignin model compounds, we utilized benzylic alcohol oxidation as a test reaction to screen the activity of all the synthesized M/CdS samples. As shown in Figure 3, upon visible light

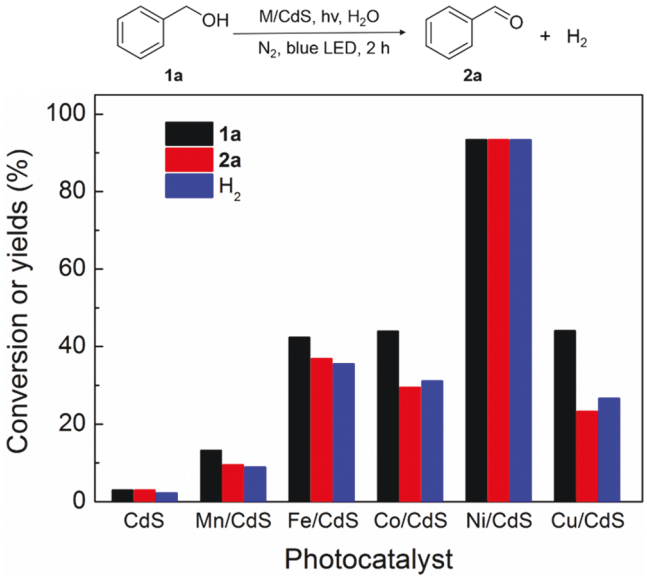

Figure 3. Activity comparison of M/CdS photocatalysts for the oxidation of benzyl alcohol, showing the conversion of benzyl alcohol together with the yields of benzaldehyde and H_2 using different photocatalysts. Conditions: 10 mM benzyl alcohol and 10 mg of photocatalyst in 10 mL of deaerated H_2O under N_2 at room temperature, illumination for 2 h.

irradiation (8 W LED, 440−460 nm) for 2 h in deaerated water, the pristine CdS nanosheets exhibited negligible activity with less than 5% conversion of benzylic alcohol and a small amount of H_2 was generated. With the decoration of first-row transition metal cocatalyts, the overall performance including benzylic alcohol conversion, benzaldehyde yield, and H_2 production was substantially increased. Among these M/CdS (M = Mn, Fe, Co, Ni, and Cu) photocatalysts, it is apparent that Ni/CdS demonstrated the best activity, achieving 93.4% conversion of benzylic alcohol (Figure 3 and Figure S15). The selectivity of benzaldehyde was nearly 100% with a reaction yield of 93.4%. In the meantime, a nearly similar yield of H_2 was obtained from Ni/CdS (Figures S16 and S17), which was also the highest yield among those obtained from all the M/CdS photocatalysts (M = Mn, Fe, Co, Ni, and Cu). It should be noted that all the generated H_2 volumes were consistent with the amounts of consumed benzyl alcohol, implying that H_2 was produced from benzyl alcohol instead of H_2O. In fact, a similar volume of H_2 could be obtained if the photocatalysis was conducted in CH_3CN as shown in Figure S18. In addition, full conversion from benzyl alcohol to benzaldehyde could be obtained by increasing the irradiation time to 2.5 h (Figure S19). It is worth mentioning that both metallic Ni and Ni^{2+} species in Ni/CdS (Figure 2f) are beneficial for the excellent photocatalytic property. It has been acknowledged that metallic Ni is an excellent H_2 evolution catalyst while oxidized Ni species can promote organic oxidation reactions.[34] Therefore, the copresence of metallic Ni and oxidized Ni is anticipated to be beneficial to the overall photocatalytic activity of H_2 evolution and benzyl alcohol oxidation. In order to further demonstrate the significant role of Ni species, a control experiment was conducted by using parent CdS which was treated with $NaBH_4$ without Ni precursor. The corresponding ^1H NMR spectra were included in Figure S20, and only a small amount of hydrobenzoin was obtained while no benzaldehyde was detected. This control experiment unambiguously proved the critical role of Ni species in the photocatalytic oxidation of benzyl alcohol to benzaldehyde on Ni/CdS. Besides the excellent activity, our Ni/CdS also exhibited robust stability. Three consecutive cycles using the same Ni/CdS photocatalyst indicated nearly no degradation during the whole process (Figure S21). Inspired by the above promising data of Ni/CdS, the following photocatalytic reactions were performed using Ni/CdS as the catalyst unless noted otherwise.

Next, we investigated the influence of the electronic effect on the photocatalytic oxidation of benzylic alcohol on Ni/CdS. A series of benzylic alcohol derivatives with either an electron-donating (−CH_3, **1b**) or an electron-withdrawing (−F, **1c**, or −CF_3, **1d**) group at the para-position were employed as the organic substrates. Since Ni/CdS was able to achieve complete benzyl alcohol oxidation within 2.5 h (Figure S19), we purposely conducted a short period (0.5 h) of photocatalytic oxidation of these benzyl alcohol derivatives on Ni/CdS. As listed in Table 1, entries 1−4 compared the yields of aldehyde and H_2 using each benzyl alcohol derivative. It was found that **1b** with the electron-donating methyl group exhibited the highest yield of 4-methylbenzaldehyde (**2b**, 54%), followed by the yield of benzaldehyde (**2a**, 46%) from the oxidation of the parent benzyl alcohol (**1a**). The installation of electron-withdrawing groups such as −F (**1c**) and −CF_3 (**1d**) apparently suppressed the reaction rate, resulting in the yields of 4-fluorobenzaldehyde (**2c**) and 4-trifluoromethylbenzaldehyde (**2d**) of 41% and 23%, respectively. The ^1H NMR and gas chromatographic (GC) spectra of these reactions after 0.5 h of photocatalysis are presented in Figures S22−S26. Figure S27 presents the yield evolution of the corresponding aldehyde of each reaction during 3 h of photocatalysis, wherein **1a**, **1b**, and **1c** were also completely transformed to their respective aldehydes while **1d** only reached a conversion of ca. 60%. Such a drastic difference in reaction rate is in good agreement with their oxidation potentials. The cyclic voltammograms of **1a**−**1d** were measured in CH_3CN and compiled in Figure S28. An irreversible oxidation potential was observed for all four compounds whose oxidation potentials follow this order: **1b** < **1a** < **1c** < **1d**. This oxidation potential trend is consistent with the aforementioned photocatalysis reaction rate. Hence, the much slower reaction rate of 4-trifluomethylbenzylic alcohol (**1d**) can be rationalized that the overall reaction was most likely driven by an outer-sphere electron transfer mechanism, similar to alcohol oxidation via redox mediators (e.g., TEMPO) while different from those reactions requiring the

DOI: 10.1021/acscatal.9b02842
ACS Catal. 2019, 9, 11341−11349

Table 1. Comparison of Photocatalytic Oxidation of Benzylic Alcohol and Its Derivatives

Entry	Substrate	Product	Organic Yield (%)	H_2 Yield (%)
1[a]	 **1a**	 **2a**	46	46
2[a]	 **1b**	 **2b**	54	54
3[a]	 **1c**	 **2c**	41	38
4[a]	 **1d**	 **2d**	23	17
5[b]	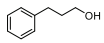 **3a**	 **4a**	0	0
6[b]	 **3b**	 **4b**	0	0
7[b]	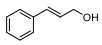 **3c**	 **4c**	90	88

[a]With 10 mM organic substrate, 10 mg of Ni/CdS in10 mL of deaerated H_2O under N_2 at room temperature, illumination for 0.5 h. [b]With 10 mM organic substrate, 10 mg of Ni/CdS in 10 mL of CH_3CN/H_2O (v/v = 9/1) under N_2 at room temperature, illumination for 24 h.

deprotonation of the alcohol group to form a metal alkoxide species as the rate-limiting step.[35] In order to further support this mechanism, a Hammett plot was conducted as shown in Figure S29. During the initial 30 min, an excellent linear relationship between benzaldehyde yield and time could be obtained (Figure S29a). From the slopes of those fitting curves, **1b** exhibited the largest rate constant of 1.780 min^{-1} and the smallest was obtained by **1d**, 0.779 min^{-1}. Overall, the reaction rates were in agreement with Hammett's relationship,[36] which has a basic equation of $\log(k/k_0) = \sigma\rho$, where k is the rate constant of the oxidation of each substituted benzyl alcohol, k_0 is the rate constant of the oxidation of parent benzyl alcohol, σ is the substituent constant and it only depends on the substituent, and ρ is the reaction constant, which only depends on the type of the reaction and not on the substituent used. By plotting log k vs σ, a straight line was obtained (Figure S29b). Such a remarkable linear relationship strongly supports the electronic effect exerted by those para substituents on the oxidation of benzyl alcohols to benzaldehydes.[37]

In addition to benzylic alcohol groups, lignin is primarily composed of three cinnamyl alcohol units, including coumaryl, coniferyl, and sinapyl alcohols. As the oxidation of the alcohol group at the C_α position (C_α−OH) is a necessity for the cleavage of the β-O-4 bond, it is highly important that a catalyst of lignin valorization expresses high selectivity for the oxidation of C_α−OH versus C_β−OH and C_γ−OH. In order to determine whether Ni/CdS's oxidation capability is selective to C_α−OH, we utilized 3-phenyl-1-propanol (**3a**) and 2-phenylethyl alcohol (**3b**) as organic substrates which bear C_γ−OH and C_β−OH groups, respectively. After 24 h of photocatalysis, no corresponding aldehydes, 3-phenylpropionaldehyde (**4a**) or phenylacetaldehyde (**4b**), were obtained (Table 1 and Figures S30−33) for the oxidation of **3a** and **3b**, suggesting that Ni/CdS was able to tolerate both C_β−OH and C_γ−OH groups. Encouraged by these results, we further expanded the alcohol scope to cinnamyl alcohol (**3c**). In addition to the terminal hydroxymethyl group, the vinyl group in **3c** is also susceptible to oxidation. The concentration evolution of cinnamyl alcohol and its oxidation products during a 24 h photocatalysis was plotted in Figure S34. The only products obtained were cinnamyl aldehyde (yield ∼ 90%) and 3-phenylpropionaldehyde (yield ∼ 10%), whose ^{1}H NMR spectra are shown in Figure S35. No vinyl oxidation products were obtained.

Photocatalytic Cleavage of Lignin Model Compounds. Encouraged by the excellent activity and selectivity toward the C_α−OH oxidation of benzylic alcohol and its derivatives on Ni/CdS, we sought to explore its photocleavage performance for a lignin model compound, 2-phenoxy-1-phenylethanol (**5**), which contains C_α−OH and an ether linkage. As shown in Figure 4a, in pure CH_3CN, complete conversion of **5** to the ketone product 2-phenoxy-1-phenylethanone (**6**) was obtained, achieving nearly 100% selectivity and yield after 18 h of photocatalysis. The ^{1}H NMR spectra of **5** before and after photocatalysis in CH_3CN are presented in Figure S36, confirming that no **5** existed post photocatalysis and the only product was **6**. In the meantime, H_2 was detected as the only reduction product. The sole oxidation product **6** allowed us to adopt subsequent chemical oxidation under ambient condition to produce benzoic acid and phenol with nearly unity yields (Figure S37), in which the C_α−C_β bond was also cleaved. By contrast, upon the addition of water, a much rapid conversion of **5** was observed in CH_3CN/H_2O (v/v = 2/8) on Ni/CdS. Figure 4b indicates that nearly complete consumption of **5** was realized within the first 8 h of photocatalysis. In addition to the ketone product **6**, directly cleaved products acetophenone (**7**) and phenol (**8**) were also obtained. Further elongating the illumination time to 18 h did not alter the relative ratio between **6**, **7**, and **8**, whose final yields were 47, 51, and 52%, respectively (Figure S38). The coproduction of **6**, **7**, and **8** with the addition of water in

DOI: 10.1021/acscatal.9b02842
ACS Catal. 2019, 9, 11341−11349

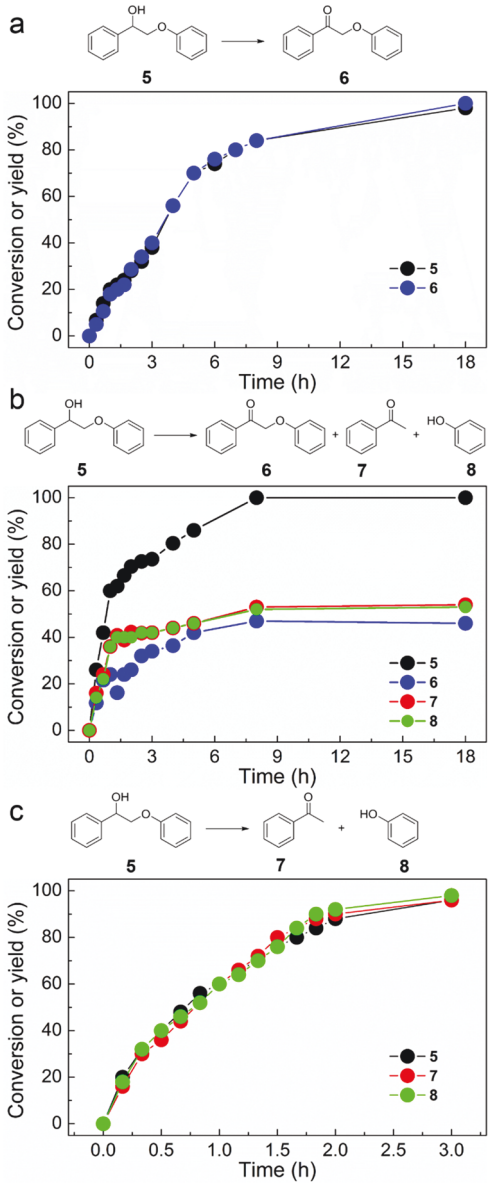

Figure 4. Conversion of substrate and yield of products over time during photocatalysis. All the photocatalytic reactions were performed with 5 mM 2-phenoxy-1-phenylethanol (**5**), 20 mg of Ni/CdS, in different deaerated solvents: (a) CH_3CN, (b) CH_3CN/H_2O (v/v = 2/8), and (c) CH_3CN/0.1 M KOH (v/v = 2/8).

CH_3CN prompted us to explore the complete photocleavage of **5** to produce **7** and **8** directly as the only products. Under alkaline conditions, a thin layer of $Ni(OH)_2$ or NiO_x may form on the surface of Ni/CdS. Those oxidized nickel species are poorer H_2 evolution catalysts compared to metallic nickel. The absorbed hydrogen species will prefer to transfer to the C_β–O bond, leading to ether bond cleavage. Indeed, as shown in Figure 4c, in a mixture of CH_3CN and 0.1 M KOH in water (v/v = 2/8), a much faster consumption rate of **5** was observed, showing complete conversion after 3 h of photocatalysis. In the meantime, the cleaved products **7** and **8** were produced immediately and reached over 90% yield within 2 h and nearly unity yields were achieved for both **7** and **8** after 3 h of photocatalysis. The HPLC spectral evolution showing the consumption of **5** and the concentration rise of **7** and **8** is presented in Figure S39. The corresponding ^1H NMR spectra of **5** before and after photocatalysis in CH_3CN/0.1 M KOH (v/v = 2/8) are shown in Figure S40, further confirming the full conversion of **5** to **7** and **8**. In order to determine the beneficial role of Ni in Ni/CdS for photocatalysis under alkaline condition, a control experiment using CdS as photocatalyst was performed. As shown in Figure S41, only cleaved products were detected; however, the reaction rate was much slower. Even after 9 h of irradiation, conversion of the lignin model was only 61%. In contrast, if Ni/CdS was used, full conversion could be achieved within 3 h under the same condition. Postphotocatalysis characterization of Ni/CdS, including SEM (Figure S42a), XRD (Figure S42b), and XPS (Figure S43) measurements, was conducted for Ni/CdS. As shown in Figures S42 and S43, our Ni/CdS maintained its nanosheet morphology and CdS wurtzite crystalline structure. The main composition still contained Cd, S, and Ni. Therefore, our Ni/CdS demonstrated strong robustness for long-term photocatalysis, in addition to its great selectivity in producing different products under different photocatalysis conditions.

Such a highly selective photocleavage performance of Ni/CdS toward the lignin model compound **5** prompted us to propose the following mechanistic steps sketched in Figure 5. Upon visible light irradiation, the excited holes generated in Ni/CdS are able to oxidize the C_α–OH group in **5** to produce the corresponding ketone product **6**. In pure CH_3CN, the great solubility of **6** would allow it to dissociate from the catalyst surface and remain as the main product. In the meantime, the extracted protons from **5** yield H_2 with the aid of Ni/CdS. However, the relatively slow conversion rate of **5** in CH_3CN implies that fast charge recombination takes place for photoirradiated Ni/CdS in CH_3CN. With the addition of water, the solubility of **6** is decreased and hence it has a better chance to linger on the surface of Ni/CdS. It should be noted that the excited electrons of Ni/CdS will facilitate the formation of adsorbed hydrogen species on the surface of Ni/CdS, which prefer to transfer to the C_β–O bond,[26] leading to ether bond cleavage and the formation of acetophenone (**7**) and phenol (**8**). Overall, the dissociation of **6** from the surface of Ni/CdS and its further cleavage compete with each other. In the mixture solvent of CH_3CN/H_2O (v/v = 2/8), a delicate balance is achieved and all the products of **6**, **7**, and **8** are obtained. However, upon the addition of 0.1 M KOH, the adsorbed hydrogen species more likely migrate to the C_β–O bond and only the directly cleaved products **7** and **8** are detected (pathway I in Figure 5). However, if the ketone product **6** is the sole product (i.e., in pure CH_3CN), a facile chemical oxidation using H_2O_2 can cleave not only the β-O-4 bond but also the C_α–C_β bond, which can lead to phenol and benzoic acid (**9**), a product not commonly observed from the direct photocleavage of lignin model compounds (pathway II in Figure 5).

In conclusion, we have reported the photocatalytic oxidation and cleavage of lignin model compounds to yield three types of products with very high selectivity on ultrathin 2D cocatalyst/CdS nanosheets. Among a series of first-row transition metal cocatalysts, including Mn, Fe, Co, Ni, and Cu, Ni/CdS exhibited the best performance for both alcohol oxidation and H_2 evolution under visible light irradiation. By judiciously modulating the solvent mixture and alkalinity, we demonstrated that it was possible to selectively achieve 2-phenoxy-1-phenylethanone from 2-phenoxy-1-phenylethanol oxidation with nearly unity yield in pure CH_3CN on Ni/CdS. A facile

DOI: 10.1021/acscatal.9b02842
ACS Catal. 2019, 9, 11341–11349

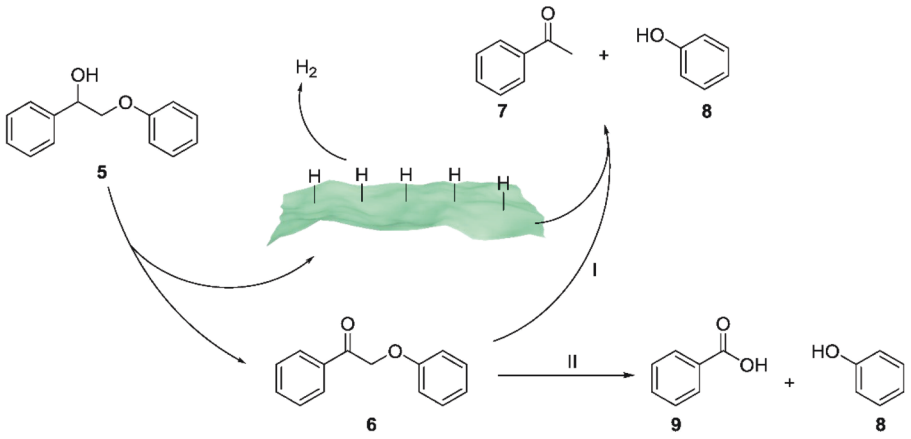

Figure 5. Proposed mechanistic steps for the two pathways of the photocatalytic oxidation of 2-phenoxy-1-phenylethanol (**5**) on Ni/CdS to produce different products with high selectivity. 2-Phenoxy-1-phenylethanone (**6**) is yielded as the sole product in CH_3CN, which will be fully transformed to acetophenone (**7**) and phenol (**8**) in CH_3CN/0.1 M KOH (v/v = 2/8) (pathway I) or benzoic acid (**9**) and phenol through a chemical oxidation (pathway II).

chemical oxidation of 2-phenoxy-1-phenylethanone could lead to the formation of benzoic acid and phenol. In contrast, photocatalysis performed in a mixture of acetonitrile and water produced 2-phenoxy-1-phenylethanone together with the direct β-O-4 cleaved products, acetophenone and phenol. Increasing pH of the solvent mixture via the addition of 0.1 M KOH could result in the complete photocleavage of 2-phenoxy-1-phenylethanol to acetophenone and phenol. A possible mechanism involving adsorbed hydrogen species on Ni/CdS during photocatalysis was proposed to rationalize the observed photocatalysis results. Overall, this work represents a rare example of controlling the photocatalytic selectivity of lignin valorization by finely tuning the reaction conditions, which is potentially applicable to other related organic transformations driven by light irradiation.

METHODS

Synthesis of CdS. A facile microwave-assisted synthesis was adopted for the preparation of ultrathin CdS nanosheets. Briefly, 0.122 g of $CdCl_2 \cdot 2.5H_2O$ was suspended in 20 mL of diethylenetriamine (DETA). After ultrasonication for about 30 min, 0.107 g of S was added and ultrasonicated for another 10 min. The resultant dark green suspension was subjected to microwave irradiation at 80 °C for 30 min. Subsequently, the obtained CdS was washed with copious amounts of methanol and water followed by centrifugation and finally dried under vacuum at room temperature.

Synthesis of M/CdS (M = Mn, Fe, Co, Ni, and Cu). A simple chemical reduction method was used for the synthesis of first-row transition metal cocatalyst decorated CdS (M/CdS). Typically, 80 mg of CdS and a certain amount of metal(II) chloride (with a molar percentage of 15%) were dispersed in 18 mL of water and sonicated for 30 min, followed by the addition of a 2 mL solution of $NaBH_4$ (0.4 M) and NaOH (2.5 M). After stirring at room temperature for 1 h, the final M/CdS samples were collected by centrifugation, washed with copious amounts of water and methanol, and dried under vacuum at room temperature.

Physical Characterization. X-ray diffraction patterns were collected on a Philips X'Pert Pro PW3040/00 (PAN analytical) instrument. The scan range was set from 10 to 90° (in 2θ) with a Cu tube operating at 45 kV and 40 mA. Scanning electron microscopy (FEI XL30, 15 kV) and transmission electron microscopy (FEI CM20, 300 kV) were used to characterize morphology of each sample. A scanning/transmission electron microscope (FEI Talos F200X) equipped with a super-EDX operating at 200 kV was used to conduct element mapping. UV−vis spectra were collected on an Agilent 8453 UV−visible spectrophotometer. An ambient McAllister scanning tunneling microscope (STM) with an R9 controller (from RHK Technologies) was used to characterize the catalyst surface with subnanometer resolution. Atomic force microscope measurements were performed in contact mode using a Bioscope scan head and motorized Digital Instruments (Bruker) backplane custom fitted to an inverted optical microscope. X-ray photoelectron spectroscopy measurements were carried out on an X-ray photoelectron spectrometer (K-alpha, Thermo Fisher Scientific, USA) using a monochromatic Al Kα X-ray source. The C 1s peak at 284.6 eV was used as an internal standard for spectral calibration. Each sample was sputtered by 1 keV Ar^+ for 60 s to remove adventitious contaminants on the surface.

Photocatalytic Experiments. Typically, a mixture of 10 mM organic substrate and 10 mg of M/CdS was thoroughly mixed in 10 mL of solvent which was charged in a 50 mL sealed round-bottom flask. The reaction mixture was deaerated with N_2 bubbling for 30 min prior to photocatalysis. Subsequently, the suspension was irradiated under royal blue light (λ = 440−460 nm) using an 8 W LED (SinkPAD-II, LuxeonStarLEDs) for a certain period.

Synthesis of 2-Phenoxy-1-phenylethanone. 2-Phenoxy-1-phenylethanone was synthesized according to a reported procedure.[38] Specifically, phenol (0.520 g, 5.5 mmol) and K_2CO_3 (1.040 g, 7.6 mmol) were mixed in 50 mL of acetone under stirring at room temperature. To the above solution, a 50 mL solution of 2-bromoacetophenone (1.000 g, 5.0 mmol) in acetone was added dropwise over 30 min. The resultant mixture was refluxed for 4 h under stirring followed by filtering and drying under vacuum. The crude product was purified by column chromatography with hexane/ethyl acetate = 20:1 and the final yield was 90%.

Chemical Cleavage of 2-Phenoxy-1-phenylethanone. 2-Phenoxy-1-phenylethanone (10.6 mg) was mixed with 0.1 mL of 30% H_2O_2 (0.88 mmol), 0.5 mL of 2.0 M NaOH (1 mmol), 0.6 mL of CH_3OH, and 0.6 mL of THF. The resultant mixture was stirred at 50 °C for 10 h, followed by acidification

DOI: 10.1021/acscatal.9b02842
ACS Catal. 2019, 9, 11341−11349

using 0.5 M HCl to pH 3. The final product was extracted with ethyl acetate and dried under vacuum with an overall yield close to 100%.

Product Quantification. The evolved H_2 from photocatalysis was quantified using gas chromatography (GC; SRI 8610C) equipped with a molecular sieve 13 packed column, a HayesSep D packed column, and a thermal conductivity detector. The oven was kept at 80 °C, and argon was used as the carrier gas. The quantity of H_2 was determined from a calibration curve using methane as an internal standard. High-performance liquid chromatography (HPLC) on a Shimadzu Prominence LC-2030C system at room temperature was used to analyze the organics. The HPLC was equipped with a UV−visible detector and a 4.6 mm × 150 mm Shim-pack GWS 5 μm C18 column. A mixture of eluting solvents (A, 5 mM ammonium acetate aqueous solution; and B, methanol) was utilized. For the separation and quantification of benzyl alcohol and benzaldehyde, the elution mixture consisted of 40% A and 60% B for each 20 min run time and the flow rate was 0.5 mL min^{-1}. For the separation and quantification of cinnamyl alcohol and cinnamaldehyde, the elution mixture consisted of 45% A and 55% B with the same flow rate. For the separation and quantification of 2-phenoxy-1-phenylethanol, 2-phenoxy-1-phenylethanone, phenol, and acetophenone, the elution mixture consisted of 20% A and 80% B and the flow rate was 1.0 mL min^{-1}. The identification and quantification of organic compounds were determined based on their corresponding standard HPLC spectra and calibration curves. ^1H NMR spectra were collected on a Bruker Advance III HD Ascend 500 MHz NMR spectrometer.

■ ASSOCIATED CONTENT

Supporting Information

The Supporting Information is available free of charge on the ACS Publications website at DOI: 10.1021/acscatal.9b02842.

Additional characterization data, including ICP, SEM, EDX, SEM, elemental mapping, XPS, AFM, STM, and CV; products analysis, including ^1H NMR, GC, and HPLC results (PDF)

■ AUTHOR INFORMATION

Corresponding Authors

*E-mail: caozhi@sxicc.ac.cn (Z.C.).
*E-mail: yujie.sun@uc.edu (Y.S.).

ORCID

David Y. Lee: 0000-0002-0494-9809
Yujie Sun: 0000-0002-4122-6255

Notes

The authors declare no competing financial interest.

■ ACKNOWLEDGMENTS

Y.S. acknowledges the financial support of Herman Frasch Foundation (820-HF17), National Science Foundation (CHE-1914546), and the University of Cincinnati. Z.C. is grateful for the financial support from the State Key Laboratory of Coal Conversion, Institute of Coal Chemistry, and Synfuels China, Co. Ltd. Z.C. also acknowledges the Hundred-Talent Program of Chinese Academy of Sciences and Shanxi Hundred-Talent Program (Y9SW911981).

■ REFERENCES

(1) Corma, A.; Iborra, S.; Velty, A. Chemical Routes for the Transformation of Biomass into Chemicals. *Chem. Rev.* **2007**, *107*, 2411−2502.
(2) Jiang, N.; You, B.; Boonstra, R.; Terrero Rodriguez, I. M.; Sun, Y. Integrating Electrocatalytic 5-Hydroxymethylfurfural Oxidation and Hydrogen Production via Co-P-Derived Electrocatalysts. *ACS Energy Lett.* **2016**, *1*, 386−390.
(3) You, B.; Jiang, N.; Liu, X.; Sun, Y. Simultaneous H_2 Generation and Biomass Upgrading in Water by an Efficient Noble-Metal-Free Bifunctional Electrocatalyst. *Angew. Chem., Int. Ed.* **2016**, *55*, 9913−9917.
(4) You, B.; Liu, X.; Jiang, N.; Sun, Y. A General Strategy for Decoupled Hydrogen Production from Water Splitting by Integrating Oxidative Biomass Valorization. *J. Am. Chem. Soc.* **2016**, *138*, 13639−13646.
(5) Brun, N.; Hesemann, P.; Esposito, D. Expanding the Biomass Derived Chemical Space. *Chem. Sci.* **2017**, *8*, 4724−4738.
(6) Xia, Q.; Chen, Z.; Shao, Y.; Gong, X.; Wang, H.; Liu, X.; Parker, S. F.; Han, X.; Yang, S.; Wang, Y. Direct Hydrodeoxygenation of Raw Woody Biomass into Liquid Alkanes. *Nat. Commun.* **2016**, *7*, 11162.
(7) Wu, X.; Fan, X.; Xie, S.; Lin, J.; Cheng, J.; Zhang, Q.; Chen, L.; Wang, Y. Solar Energy-Driven Lignin-First Approach to Full Utilization of Lignocellulosic Biomass under Mild Conditions. *Nat. Catal.* **2018**, *1*, 772−780.
(8) Li, K.; Sun, Y. Electrocatalytic Upgrading of Biomass-Derived Intermediate Compounds to Value-Added Products. *Chem. - Eur. J.* **2018**, *24*, 18258−18270.
(9) Gilkey, M. J.; Xu, B. Heterogeneous Catalytic Transfer Hydrogenation as an Effective Pathway in Biomass Upgrading. *ACS Catal.* **2016**, *6*, 1420−1436.
(10) Li, S.-H.; Liu, S.; Colmenares, J. C.; Xu, Y.-J. An Approach for Lignin Valorization by Heterogeneous Photocatalysis. *Green Chem.* **2016**, *18*, 594−607.
(11) Hanson, S. K.; Baker, R. T. Knocking on Wood: Base Metal Complexes as Catalysts for Selective Oxidation of Lignin Models and Extracts. *Acc. Chem. Res.* **2015**, *48*, 2037−2048.
(12) Rinaldi, R.; Jastrzebski, R.; Clough, M. T.; Ralph, J.; Kennema, M.; Bruijnincx, P. C. A.; Weckhuysen, B. M. Paving the Way for Lignin Valorization: Recent Advances in Bioengineering, Biorefining and Catalysis. *Angew. Chem., Int. Ed.* **2016**, *55*, 8164−8215.
(13) Son, S.; Toste, F. D. Non-Oxidative Vanadium-Catalyzed C-O Bond Cleavage: Application to Degradation of Lignin Model Compounds. *Angew. Chem., Int. Ed.* **2010**, *49*, 3791−3794.
(14) Zakzeski, J.; Bruijnincx, P. C.; Jongerius, A. L.; Weckhuysen, B. M. The Catalytic Valorization of Lignin for the Production of Renewable Chemicals. *Chem. Rev.* **2010**, *110*, 3552−3599.
(15) Li, C.; Zhao, X.; Wang, A.; Huber, G. W.; Zhang, T. Catalytic Transformation of Lignin for the Production of Chemicals and Fuels. *Chem. Rev.* **2015**, *115*, 11559−11624.
(16) Kim, S.; Chmely, S. C.; Nimlos, M. R.; Bomble, Y. J.; Foust, T. D.; Paton, R. S.; Beckham, G. T. Computational Study of Bond Dissociation Enthalpies for a Large Range of Native and Modified Lignins. *J. Phys. Chem. Lett.* **2011**, *2*, 2846−2852.
(17) Ma, R.; Hao, W.; Ma, X.; Tian, Y.; Li, Y. Catalytic Ethanolysis of Kraft Lignin into High-Value Small-Molecular Chemicals over a Nanostructured α-Molybdenum Carbide Catalyst. *Angew. Chem., Int. Ed.* **2014**, *53*, 7310−7315.
(18) Zhu, R.; Wang, B.; Cui, M.; Deng, J.; Li, X.; Ma, Y.; Fu, Y. Chemoselective Oxidant-Free Dehydrogenation of Alcohols in Lignin Using Cp* Ir Catalysts. *Green Chem.* **2016**, *18*, 2029−2036.
(19) Li, C.; Zhao, X.; Wang, A.; Huber, G. W.; Zhang, T. Catalytic Transformation of Lignin for the Production of Chemicals and Fuels. *Chem. Rev.* **2015**, *115*, 11559−11624.
(20) Lancefield, C. S.; Ojo, O. S.; Tran, F.; Westwood, N. J. Isolation of Functionalized Phenolic Monomers through Selective Oxidation and C-O Bond Cleavage of the β-O-4 Linkages in Lignin. *Angew. Chem., Int. Ed.* **2015**, *54*, 258−262.

DOI: 10.1021/acscatal.9b02842
ACS Catal. 2019, 9, 11341−11349

(21) Rahimi, A.; Azarpira, A.; Kim, H.; Ralph, J.; Stahl, S. S. Chemoselective Metal-Free Aerobic Alcohol Oxidation in Lignin. *J. Am. Chem. Soc.* **2013**, *135*, 6415−6418.
(22) Nguyen, J. D.; Matsuura, B. S.; Stephenson, C. R. A Photochemical Strategy for Lignin Degradation at Room Temperature. *J. Am. Chem. Soc.* **2014**, *136*, 1218−1221.
(23) Kärkäs, M. D.; Bosque, I.; Matsuura, B. S.; Stephenson, C. R. Photocatalytic Oxidation of Lignin Model Systems by Merging Visible-Light Photoredox and Palladium Catalysis. *Org. Lett.* **2016**, *18*, 5166−5169.
(24) Bosque, I.; Magallanes, G.; Rigoulet, M.; Kärkäs, M. D.; Stephenson, C. R. Redox Catalysis Facilitates Lignin Depolymerization. *ACS Cent. Sci.* **2017**, *3*, 621−628.
(25) Colmenares, J. C. Nanophotocatalysis in Selective Transformations of Lignocellulose-derived Molecules: A Green Approach for the synthesis of Fuels, Fine Chemicals, and Pharmaceuticals. In *Green Photo-active Nanomaterials: Sustainable Energy and Environmental Remediation*; Nuraje, N., Asmatulu, R., Mul, G., Eds.; The Royal Society of Chemistry: 2015; pp 168−201.
(26) Luo, N.; Wang, M.; Li, H.; Zhang, J.; Hou, T.; Chen, H.; Zhang, X.; Lu, J.; Wang, F. Visible-Light-Driven Self-Hydrogen Transfer Hydrogenolysis of Lignin Models and Extracts into Phenolic Products. *ACS Catal.* **2017**, *7*, 4571−4580.
(27) Setzler, B. P.; Zhuang, Z.; Wittkopf, J. A.; Yan, Y. Activity Targets for Nanostructured Platinum-Group-Metal-Free Catalysts in Hydroxide Exchange Membrane Fuel Cells. *Nat. Nanotechnol.* **2016**, *11*, 1020−1025.
(28) Vojvodic, A.; Medford, A. J.; Studt, F.; Abild-Pedersen, F.; Khan, T. S.; Bligaard, T.; Nørskov, J. K. Exploring the Limits: A Low-Pressure, Low-Temperature Haber-Bosch Process. *Chem. Phys. Lett.* **2014**, *598*, 108−112.
(29) Han, G.; Jin, Y.-H.; Burgess, R. A.; Dickenson, N. E.; Cao, X.-M.; Sun, Y. Visible Light-Diven Valorization of Biomass Intermediates Integrated with H_2 Production Catalyzed by Ultrathin Ni/CdS Nanosheets. *J. Am. Chem. Soc.* **2017**, *139*, 15584−15587.
(30) Kim, Y.; Kim, H. B.; Jang, D. J. Facile Microwave Fabrication of CdS Nanobubbles with Highly Efficient Photocatalytic Performances. *J. Mater. Chem. A* **2014**, *2*, 5791−5799.
(31) Miao, J.; Xiao, F.-X.; Yang, H. B.; Khoo, S. Y.; Chen, J.; Fan, Z.; Hsu, Y.-Y.; Chen, H. M.; Zhang, H.; Liu, B. Hierarchical Ni-Mo-S Nanosheets on Carbon Fiber Cloth: AFlexible Electrode for Efficient Hydrogen Generation in Neutral Electrolyte. *Sci. Adv.* **2015**, *1*, No. e1500259.
(32) Pan, Y.; Liu, Y.; Zhao, J.; Yang, K.; Liang, J.; Liu, D.; Hu, W.; Liu, D.; Liu, Y.; Liu, C. Monodispersed Nickel Phosphide Nanocrystals with Different Phases: Synthesis, Characterization and Electrocatalytic Properties for Hydrogen Evolution. *J. Mater. Chem. A* **2015**, *3*, 1656−1665.
(33) You, B.; Jiang, N.; Sheng, M.; Bhushan, M. W.; Sun, Y. Hierarchically Porous Urchin-Like Ni_2P Superstructures Supported on Nickel Foam as Efficient Bifunctional Electrocatalysts for Overall Water Splitting. *ACS Catal.* **2016**, *6*, 714−721.
(34) You, B.; Liu, X.; Liu, X.; Sun, Y. Efficient H_2 Evolution Coupled with Oxidative Refining of Alcohols via a Hierarchically Porous Nickel Bifunctional Electrocatalyst. *ACS Catal.* **2017**, *7*, 4564−4570.
(35) Rahimi, A.; Ulbrich, A.; Coon, J. J.; Stahl, S. S. Formic-Acid-Induced Depolymerization of Oxidized Lignin to Aromatics. *Nature* **2014**, *515*, 249.
(36) Hammett, L. P. The Effect of Structure Upon the Reactions of Organic Compounds. Benzene Derivatives. *J. Am. Chem. Soc.* **1937**, *59*, 96−103.
(37) Yurdakal, S.; Palmisano, G.; Loddo, V.; Alagöz, O.; Augugliaro, V.; Palmisano, L. Selective Photocatalytic Oxidation of 4-Substituted Aromatic Alcohols in Water with Rutile TiO_2 Prepared at Room Temperature. *Green Chem.* **2009**, *11*, 510−516.
(38) Zhang, J. W.; Lu, G. P.; Cai, C. Self-Hydrogen Transfer Hydrogenolysis of β-O-4 Linkages in Lignin Catalyzed by MIL-100 (Fe) Supported Pd-Ni BMNPs. *Green Chem.* **2017**, *19*, 4538−4543.

DOI: 10.1021/acscatal.9b02842
ACS Catal. 2019, 9, 11341−11349